Progress In Electromagnetics Research, Vol. 148, 141–150, 2014

Inhomogeneous Microwave Lens Based on Periodically Loaded Transmission Lines

Joni Vehmas[1, *], Pekka Alitalo[2], and Sergei Tretyakov[1]

Abstract—A new design for a low-reflection inhomogeneous microwave lens based on periodically loaded one-dimensional transmission lines is proposed and experimentally tested. The inhomogeneous effective refractive index of this flat-profile lens is achieved by loading the transmission lines comprising the lens with different inductive elements.

1. INTRODUCTION

Dielectric lenses, both homogeneous and inhomogeneous, have been commonly used in microwave applications, for example for antenna phase correction and wide-angle scanning (e.g., [1]). However, these lenses have several drawbacks such as having poor impedance matching to free space leading to considerable reflections and unwanted loss of power, dielectric losses and requiring possibly complex shaping of the lens contour. In contrast to optical lenses, the use of anti-reflection coatings in microwave lenses is usually not practical due to their large thickness, weight, and cost. Several alternative ways for realizing inhomogeneous microwave lenses have been suggested. Especially, Luneburg lenses have been of interest lately. For example, the inhomogeneous refractive index of the Luneburg lens has been realized by drilling electrically small holes into a dielectric [2], by using pressed foam material [3], and by employing several homogeneous shells [4]. On the other hand, the use of metamaterials with negative refractive index for creating a microwave lens has also been discussed recently in [5, 6]. Transformation optics techniques can also be utilized in order to achieve inhomogeneous refractive index for the lens as was shown in [7], where a planar hyperbolic lens was fabricated using liquid phase vacuum casting. An original approach to realizing a well-matched microwave lens was suggested and studied numerically in [8, 9]. That design, which is based on two-dimensional or three-dimensional transmission-line (TL) networks, has the benefit of having very good impedance matching with free space as well as being fairly easy to manufacture. Independent control of both refractive index and wave impedance becomes possible without any magnetic insertions, simply using appropriate bulk periodical loads in the transmission lines and by tuning the impedance of the host transmission lines themselves [10–12]. A similar design was also used for realizing a Luneburg lens antenna in [13]. Recently, another waveguide-based microwave lens was suggested and studied numerically in [14]. In that lens design, a slab of stacked near cut-off rectangular waveguides emulating ϵ-near-zero (ENZ) media is designed to behave as a bi-concave symmetric lens.

In this paper, we propose and test experimentally a new microwave lens design based on the use of loaded one-dimensional transmission lines. The proposed lens is a converging lens and has a flat profile (as opposed to a curved one as in the lenses based on TL networks [8, 9]) with inhomogeneous index of refraction in the direction orthogonal to the optical axis. A linear metal taper is used for coupling the incident wave from free space to the TLs and vice versa (as in e.g., [15]). The main benefits of the new

Received 13 May 2014, Accepted 18 June 2014, Scheduled 24 July 2014

* Corresponding author: Joni Vehmas (joni.vehmas@aalto.fi).

[1] Department of Radio Science and Engineering, Aalto University, P. O. Box 13000, Aalto FI-00076, Finland. [2]Finnish Patent and Registration Office, P. O. Box 1140, Helsinki FI-00101, Finland.

lens design, as compared to traditional homogeneous dielectric lenses [1] or the previously studied TL and waveguide lenses [8, 9, 14], are fairly simple and cheap manufacturing requiring only well-established manufacturing techniques and simple reconfigurability of the refractive index (via change of loading inductances). An initial numerical study of the proposed TL lens was presented in [16].

2. LENS DESIGN

The proposed microwave lens consists of a set of parallel, periodically loaded one-dimensional (1D) TLs with different loading elements and two so-called transition layers on each side of the TL array. The transmission lines, which are common parallel strip lines, are loaded periodically with inductive meander line elements. The transition layers, on the other hand, are simple metal tapers, similar to the ones used in [15]. The phase of the incident wave is modified using the TLs with different loading elements while the transition layers are used just for coupling the incident wave to the TLs and back to free space. The lens can be made volumetric by stacking several sets of such arrays of 1D-TLs and transition layers on top of each other, again, similar to the volumetric cloak structure of [15]. The basic structure of the lens and its operating principle are illustrated in Fig. 1.

As the profile of the lens is flat, the effective refractive index of the TLs must be varied in order to ensure the desired phase variation in the output plane. Instead of having a set of homogeneous TLs each filled with different materials with slightly different refractive indices, this is achieved simply by varying the dimensions of the distributed inductive loading elements. The dimensions of the host TL are the same for all lines.

According to the basic design equations for microwave waveguide lenses which focus plane waves into a point (e.g., [1]), the required refractive index profile has the form

$$n(\rho) = n_0 - \frac{1}{d}\left[\sqrt{F^2 + \rho^2} - F\right], \tag{1}$$

where n_0 is the refractive index at the lens center, d the thickness of the lens, F the distance between the source (or the focus) and the lens, and ρ the distance from the lens center. Notably, (1) does not depend on the frequency, thus, ideally, the designed lens should have a very wide bandwidth. However, the TL implementation limits the bandwidth to frequencies where the period of the loaded TLs is sufficiently small electrically so that the effective refractive indices of the TLs are approximately dispersionless.

In our lens design, we have $n_0 = 1.725$ while the dimensions of the lens have been chosen so that at the main operational frequency of 3 GHz $F = 10\,\mathrm{cm} = \lambda$ and $d = 18.5\,\mathrm{cm} = 1.85\lambda$. We use nine different inductive meander line loading elements in order to approximate the smoothly varying ideal refractive index profile. Altogether, the lens consists of 72 TL-branches so that four TLs with the same

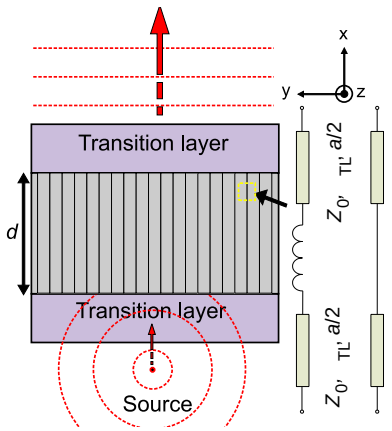

Figure 1. Basic lens setup. The vertical lines show the positions of 1D-TLs loaded with meander inductances, with the equivalent circuit of unit cells shown in the inset.

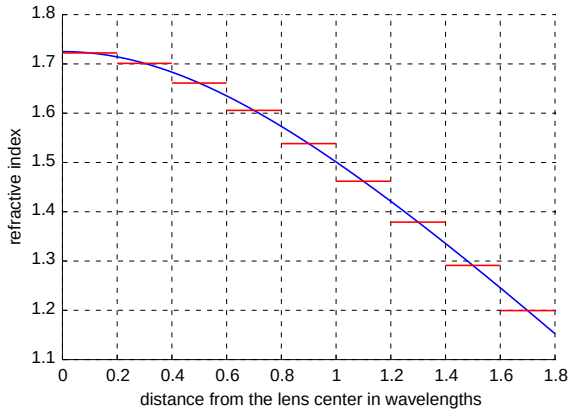

Figure 2. Ideal refractive index profile (blue solid line) and the refractive index profile of the proposed lens (red line segments).

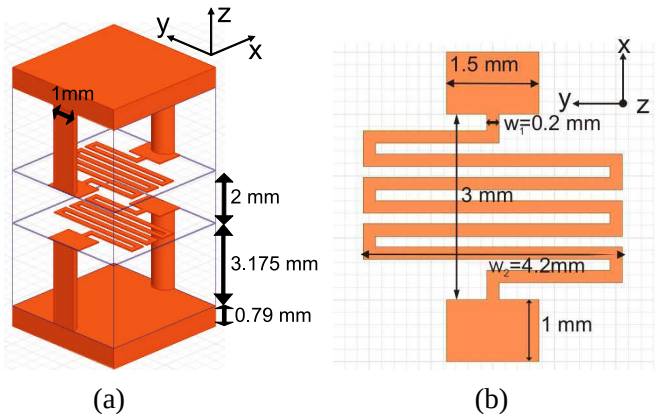

Figure 3. Unit cell for the loaded TL with the highest effective refractive index ($n = 1.72$). The dielectrics (top/bottom: Rogers Duroid 5870, middle: Rohacell 71 WF) are rendered invisible for clarity. The TL metalization thickness is 35 µm.

Table 1. Dimensions of the inductive elements and effective refractive indices for each loaded TL. Other dimensions are according to Fig. 3 for all elements.

	TL_1	TL_2	TL_3	TL_4	TL_5	TL_6	TL_7	TL_8	TL_9
n	1.20	1.29	1.38	1.46	1.54	1.61	1.66	1.70	1.72
w_1 [mm]	0.32	0.2	0.2	0.2	0.2	0.2	0.2	0.2	0.2
w_2 [mm]	0.32	0.92	1.5	2.08	2.6	3.18	3.6	3.98	4.2

loading element are always placed side by side (making the period of the structure $a = 5$ mm and the total width of the lens 36 cm = 3.6λ at 3 GHz). The length of the transition layers is 6 cm. The ideal refractive index profile as well as the refractive index profile of the proposed lens are shown in Fig. 2. The design procedure for the inductive loading elements is described in detail in [16]. The unit cell corresponding to the highest refractive index is shown in Fig. 3. The dimensions for the rest of the meander line elements are shown in Table 1.

3. NUMERICAL RESULTS

3.1. Reflection from the Lens

The proposed lens was previously studied numerically in [16]. In that paper, it was shown that the losses of the lens are small and fairly low reflection can be achieved. However, as the effective refractive index is different for each TL, the thickness resonances of the structure are also different for different TLs. This means that the reflection coefficient cannot be perfectly minimized for all TLs simultaneously. Still, the reflection for all TLs is below −7 dB near the design frequency (2.5 GHz–3.5 GHz) with the average reflection coefficient at 3 GHz being −11.6 dB. The lens was designed so that the reflection in the middle of the lens is minimized ($|\Gamma| < -14.7$ dB for the 24 TLs in the middle of the lens). In comparison, the reflection for a dielectric slab of the same size with refractive index 1.72 is −6.7 dB. With higher refractive indices, the TL lens is expected to more clearly outperform its dielectric counterpart [8, 9]. Such higher refractive indices would require higher loading inductances but would be realizable by using, e.g., lumped inductors. Here, we wanted to limit the loading elements to simple inductors for simplicity. By introducing additional capacitor loading, the impedance of each line could be tuned and thus the reflection could also be improved. Simulated reflection and transmission coefficients for all the different TLs in the bandwidth of 2.5 GHz–3.5 GHz are shown in [16].

3.2. Dispersion of the TLs

It was said previously that the dispersion of the meander lines limits the operational bandwidth of the lens. A transmission line loaded periodically with dispersive loads (capacitors and/or inductors) is always dispersive. The amount of dispersion depends not only on the period of the structure and frequency but also on the loading element and properties of the unloaded TL. Here, we will study the effect of dispersion on the refractive index of each TL and on the phase front on the backside of the lens. The refractive index for each TL was calculated separately using Ansys HFSS. In these simulations, the lens was assumed to be infinitely periodic in the y-direction. The resulting refractive indices are shown in Fig. 4. Clearly, as the inductance of the meander line increases, so does the dispersion of the effective refractive index. For the TL loaded with the meander line with the lowest inductance, the corresponding TL is almost dispersionless in the studied frequencies while the refractive index of the TLs with the highest refractive index changes from 1.71 to 2.01 as frequency changes from 2 GHz to 7 GHz. In other words, the fields propagating in the middle of the lens encounter an extra phase shift compared to the ideal dispersionless case which increases with frequency.

The described dispersion behavior can be easily understood by theoretically studying the propagation in such a TL structure. The dispersion for a TL loaded periodically with series inductors can be easily derived using ABCD matrices and the Floquet theorem [18] and is given by

$$\cos(\beta a) = \cos(\beta_{\mathrm{TL}} a) - \frac{\omega L}{2Z_0}\sin(\beta_{\mathrm{TL}} a), \tag{2}$$

where β is the propagation constant of the loaded TL, β_{TL} the propagation constant of the unloaded TL, a is the period, ω the angular frequency, L the inductance of the loading inductor, and Z_0 the characteristic impedance of the unloaded TL. If the period is small enough so that we have $\beta_{\mathrm{TL}} a \ll 1$ and $\beta a \ll 1$, (2) simplifies to a dispersionless equation

$$\beta = \beta_{\mathrm{TL}}\sqrt{1 + \frac{L}{Z_0 a\sqrt{\epsilon\mu}}}, \tag{3}$$

where ϵ and μ are the effective permittivity and permeability of the unloaded TL, respectively. As β depends also on the inductance of the loading inductor, this inductance (along with the TL parameters β_{TL} and Z_0 which are the same for all the TLs in our case) essentially determines how small the period must be in order to have negligible dispersion.

Another way to look at this is to study the phase of the signal on the backside of the lens at the end of each TL when the structure is fed, as shown in Fig. 1, with a cylindrical wave source positioned 10 cm away from the TL array of the lens. Ideally, the phase should be uniform, as a plane wave should be generated behind the lens. The maximal phase difference between the fields at the end of each TL

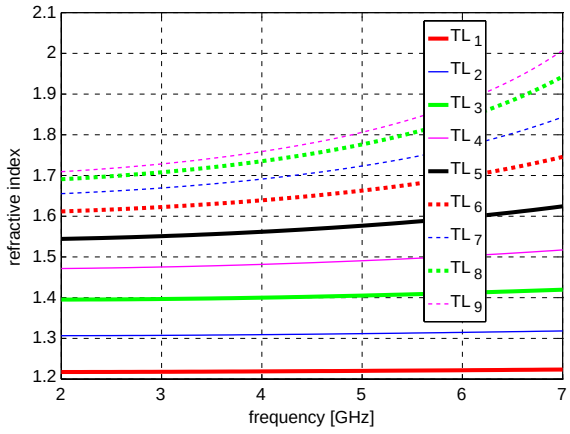

Figure 4. Refractive index of each TL, as defined in Table 1, as a function of frequency.

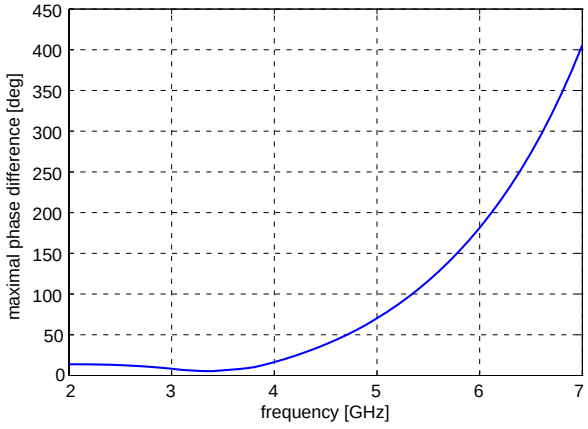

Figure 5. Maximal phase difference on the backside of the lens.

(in practice, the phase difference between the middle TLs and the outer TLs) estimated based on the refractive indices of Fig. 4 is shown in Fig. 5. Firstly, we can see that the effect of dispersion is fairly small, less than 15°, below 3.9 GHz. As the frequency increases above 3.9 GHz, the effect of dispersion increases quite rapidly and due to this, the lens effectively stops working. In conclusion, the dispersion limits operating bandwidth of the lens at high frequencies so that only frequencies below 4 GHz provide appropriate lensing.

4. MEASUREMENTS

4.1. Manufactured Prototype

One layer of the TL-lens with the dimensions and material properties as described in the previous sections was manufactured in two parts. Firstly, the top and bottom dielectric-backed metal (copper) strips comprising the TLs were manufactured using Printed Circuit Board (PCB) technology with the used substrate being Rogers Duroid 5870 as in the simulations. As described earlier, the two sets of strips are separated by a 2 mm-thick slab of Rohacell 71 WF ($\epsilon_r = 1.07$) with the same horizontal dimensions as the whole lens without the transition layers. Secondly, the transition layers as well as the thin metal sheets situated above the top PCB and under the bottom PCB were machined out of aluminum. The transition layer tapers were attached to the metal sheets using screws. The two manufactured PCBs were each placed between the transition layer tapers and secured in place with epoxy glue. The TLs were connected to the transition layers using silver paint and silver epoxy. In order to make sure that the connection was perfect, a piece of a copper tape was placed into each gap between the PCB and the transition layers. One half of the manufactured lens, i.e., the transition layers connected to the metal-backed PCB, can be seen in Fig. 6.

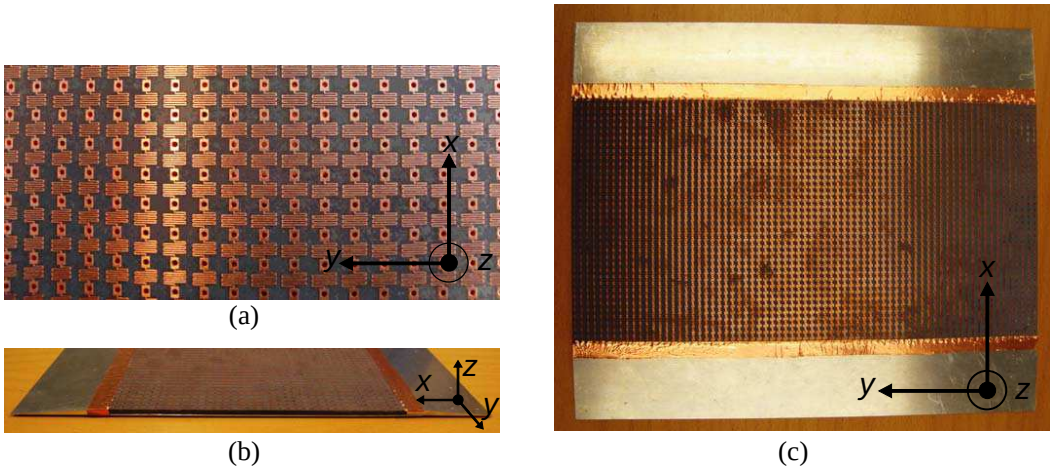

Figure 6. (a) Close-up of the TLs loaded with meander line elements; one half of the manufactured lens (excluding the middle Rohacell sheet) (b) from the side and (c) from above.

4.2. Measurement Setup

The operation of the TL-lens was verified by conducting a measurement inside a parallel-plate waveguide. By placing a single layer of the TL-lens inside a parallel-plate waveguide with the same height as the lens, we can effectively simulate the free-space scenario where the lens is infinitely periodic in the vertical direction. The measurement itself is similar to the one conducted in [17]. A parallel-plate waveguide with the dimensions 90 cm × 80 cm and the height of 1 cm is fed with a stationary vertical coaxial feed from the center of one of its shorter sides. The inner conductor of the feed (the length 1 cm) is connected to the bottom plate of the waveguide and the outer conductor to the top plate. The manufactured single-layer lens is positioned 4 cm away from the feed, parallel to the edge of the waveguide (as in the

earlier numerical/semi-analytical analysis). As the length of the transition layers is 6 cm, the array of TLs is, thus, positioned 10 cm (= focal length of the lens at 3 GHz) away from the lens. The electric field distribution behind the lens is measured through a 25 cm × 35 cm copper mesh embedded to the bottom plate of the waveguide using a movable, vertical coaxial probe positioned about 1 cm under the mesh. The period and the wire thickness of the mesh are 0.5 cm and 1 mm, respectively. The mesh is positioned 34.5 cm (= 4 cm + lens thickness) away from the source and in the center of the waveguide in the orthogonal (y-) direction. A quarter wave sleeve balun (operational frequency 3 GHz) is used in the coaxial probe in order to prevent field coupling to the outer conductor of the coaxial line. The mesh is surrounded with microwave absorbing material in order to reduce reflections from the edges of the waveguide. Additional absorbers are positioned under the parallel-plate waveguide between the feed and the probe in order to prevent direct coupling between them. The stationary transmitting feed is connected to port 1 of Agilent Technologies' E8363A vector network analyzer (VNA) via a 22 dB amplifier, while the probe is connected to port 2.

A field scanning system consisting of a PC connected to two moving platforms (for x- and y-directions) manufactured by Physik Instrumente and the aforementioned VNA was used to scan the field under the mesh in the horizontal plane. In other words, the field scanning system was used to move the probe horizontally according to a predefined measurement pattern measuring S_{21} automatically at each of the defined measurement points. The size of the scanned area was 22 cm × 29 cm, and it was positioned approximately in the center of the metal mesh. The rectangular sweep consisted of 23 × 30 points making the period 1 cm. The measured frequency range was 1 GHz–10 GHz with 1801 frequency points. The corresponding field scan was also conducted for the waveguide without the lens. A schematic of the measurement setup can be seen in Fig. 7(a) and the parallel-plate waveguide of the actual measurement setup with the top plate removed in Fig. 7(b).

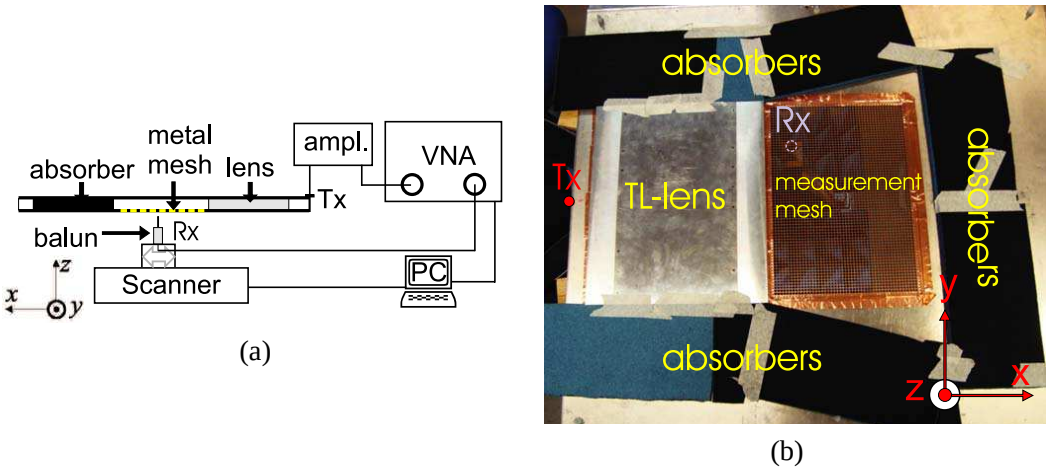

Figure 7. (a) Schematic of the measurement setup (dimensions not in scale); (b) parallel-plate waveguide including the lens from above with top plate of the waveguide removed.

4.3. Data Processing

Even though microwave absorbers were used for eliminating reflections from the edges of the waveguide, there were still considerable reflections inside the waveguide from the absorbers themselves. This is partly due to the fact that the electrical size of the parallel-plate waveguide is only moderately large at the studied frequencies (approx. $9\lambda \times 8\lambda$ at 3 GHz). This is a problem especially when measuring the waveguide without the lens as the lens "captures" a large part of the waves that would otherwise be reflected from the edges of the waveguide or absorbers. Also, as the behavior of each of the TLs comprising the lens was simulated previously in [16] and no strong multiple reflections were detected, we can safely assume that the delayed wave components are due to the setup itself and not due to the lens. In order to get rid of these parasitic signals, post-processing in the form of time-gating was used.

First, the measured S_{21} was converted into time-domain using Inverse Fast Fourier Transform. Then, the maximum of the signal amplitude was found. It was assumed that this maximum corresponded to the wanted signal and a time window function was assigned around this maximum point. Tukey window (also known as the tapered cosine window) was used with the window parameter $\alpha = 0.5$. Tukey window has the form [19]

$$w(n) = \begin{cases} \frac{1}{2}\left[1 + \cos\left(\pi\left(\frac{2n}{\alpha(N-1)} - 1\right)\right)\right] & \text{for } 0 \le n \le \frac{\alpha(N-1)}{2} \\ 1 & \text{for } \frac{\alpha(N-1)}{2} \le n \le (N-1)\left(1 - \frac{\alpha}{2}\right) \\ \frac{1}{2}\left[1 + \cos\left(\pi\left(\frac{2n}{\alpha(N-1)} - \frac{2}{\alpha} + 1\right)\right)\right] & \text{for } (N-1)(1-\frac{\alpha}{2}) \le n \le (N-1). \end{cases} \quad (4)$$

Here, N is the width of the window (in samples) and parameter α is defined as the ratio of taper to constant sections with $\alpha = 1$ corresponding to rectangular window and $\alpha = 0$ corresponding Hann window. This particular window function was chosen as we wanted to minimize distortion of the main signal (i.e., energy loss) due to time-gating (even if that meant that some of the parasitic signals would still be included). Moreover, we did not want to use the rectangular time window function as it can be considered non-physical with its corresponding frequency spectrum (sinc function) spreading to infinity. For the measurement without the lens, a time window of 1.55 ns (15 points) around the maximum was used. For the lens case, larger window of 2.92 ns (19 points) was used as it was expected that the signal would be more spread out in this case. Also, the effect of time-gating in this case was much smaller compared to the empty waveguide case as reflected signals were not as big of a problem. Finally, the signal was converted back to the frequency domain using Fast Fourier Transform.

4.4. Measurement Results

The real part of the complex electric field normalized to the input signal (i.e., the real part of the measured S_{21}) at 3 GHz when the TL-lens is placed in front of the feed and when the waveguide is empty can be seen in Fig. 8. Here, basic linear interpolation is used for getting a smoothly varying field pattern from the set of discrete measurement points. In the empty waveguide case, we can see cylindrical wavefronts propagating from the source, as expected. On the other hand, when the lens is placed inside the waveguide, the field distribution is clearly close to the desired plane-wave distribution. Also, the magnitude of the measured S_{21} is larger with the lens than with the empty waveguide which indicates that the lens does not cause considerable loss of power due to reflections or dielectric losses. Even though the lens does properly modify the wavefront and the response is quite close to a plane wave, the wavefronts are still slightly curved, especially near the center. This may be due to inaccuracies in manufacturing or in optimizing the meander line dimensions in order to achieve the wanted refractive

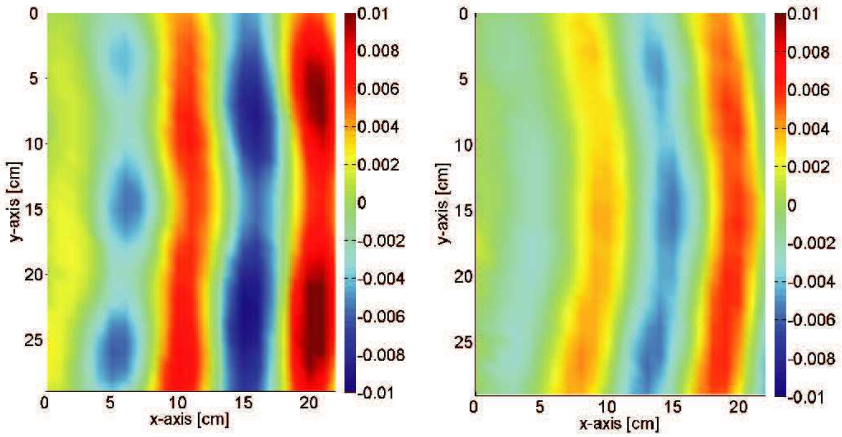

Figure 8. Measured real part of the complex electric field normalized to the input signal (S_{21}) at 3 GHz (a) with the lens and (b) without the lens.

indices. In the unit cell simulations, to simplify the calculations it was assumed that the structure is infinitely periodic (both in the propagation direction and in the orthogonal directions) which is obviously not the case in reality. Even a small change of the effective refractive index of the TL can change the transmission phase considerably. Better results could be achieved by optimizing a full model of the lens numerically instead of optimizing each individual TL separately. Unfortunately, this was not an option here due to demands of such large computation. However, the phase error can be compensated quite well by simply moving the lens. By placing the lens 1.5 cm closer to the feed, an improved plane wave is achieved as shown in Fig. 9. Notably, the electric field closer to the feed appears in all the studied cases weaker than the field farther away from the feed. This is probably due to the measurement setup itself, e.g., due to scattering from the boundary between the regular waveguide and the metal grid.

The lens was designed to work at 3 GHz, but the operation of the lens was also studied at other frequencies. Due to the limitations of the measurement setup (e.g., the limited size of the parallel-plate waveguide), frequencies lower than approximately 2.6 GHz (or even higher for the empty waveguide case) could not be measured accurately. However, at 2.6 GHz, as can be seen from Fig. 10, the lens works as expected generating a plane wave. For this measurement, a much wider time window of 29.2 ns was used as the smaller window was observed to distort the signal and decrease its amplitude considerably

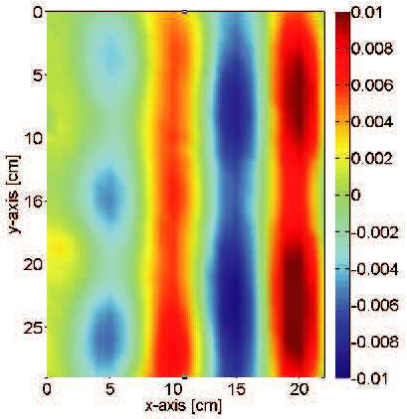

Figure 9. Measured real part of the complex electric field normalized to the input signal (S_{21}) with the lens at 3 GHz when the lens is moved 1.5 cm closer to the feed in order to compensate for the observed phase error.

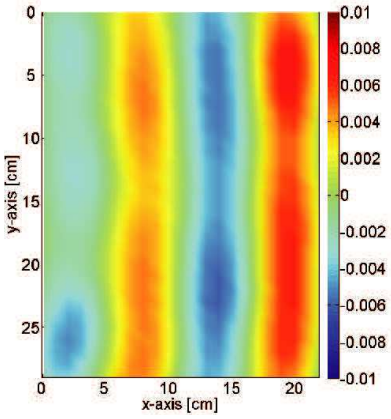

Figure 10. Measured real part of the complex electric field normalized to the input signal (S_{21}) with the lens at 2.6 GHz.

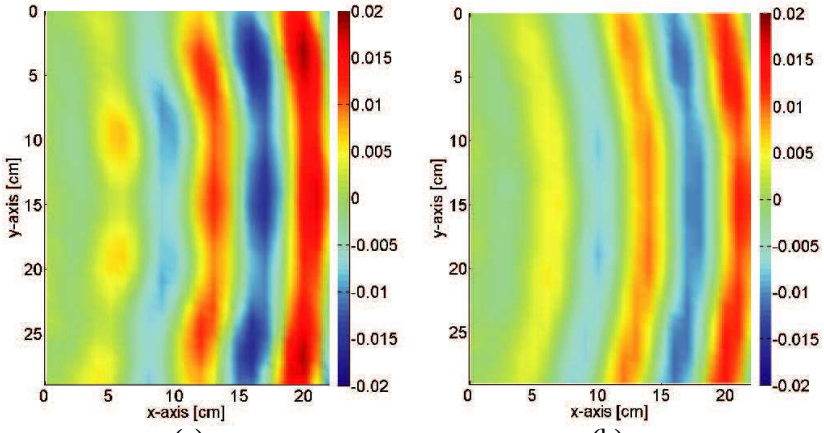

Figure 11. Measured real part of the complex electric field normalized to the input signal (S_{21}) at 4 GHz (a) with the lens and (b) without the lens.

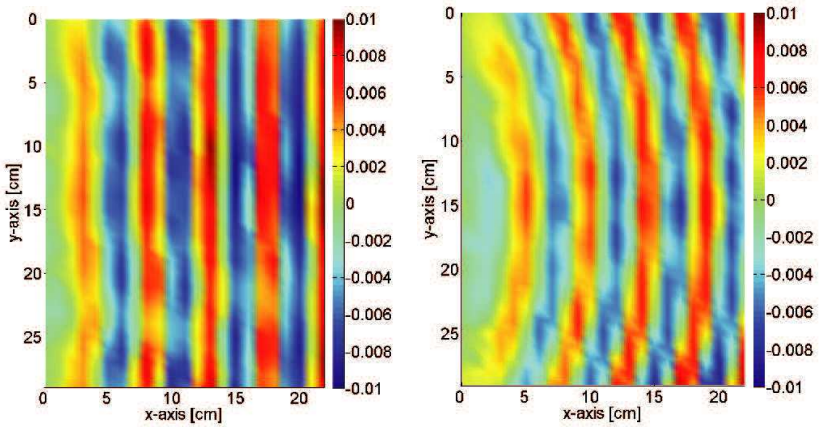

Figure 12. Measured real part of the complex electric field normalized to the input signal (S_{21}) at 6.5 GHz (a) with the lens and (b) without the lens.

at such low frequency (compared to the case without any time-gating). The corresponding result for the empty waveguide could not be extracted correctly from the measurements at this frequency due to considerable reflections from the absorbers inside the waveguide which could not be eliminated with time-gating without distorting the signal. As the dispersion is expected to be small at frequencies smaller than 2.6 GHz according to Fig. 11, we can expect the lens to also work at these frequencies. At frequencies higher than 3 GHz, there is no problem with the measurement setup though the dispersion of the meander line elements starts to limit the performance considerably as was shown earlier numerically in Fig. 5. At 4 GHz, the field is already considerably distorted as can be seen from Fig. 11. By reducing the electrical size of the unit cell the dispersion of the TLs could be reduced and thus the operational bandwidth of the lens increased though this would make the manufacturing of the lens more difficult and the simulations for the whole lens even more computationally demanding. Interestingly, at 6.5 GHz the lens does, however, appears to work quite well as can be seen from Fig. 12 even though the dispersion of the TLs is already very large at this frequency. This only happens at this one higher frequency. This is most likely due to the phase error between the middle TLs (with high dispersion) and outer TLs (with little dispersion) reaching 360° (or even more) so that most of the TLs are approximately in phase. According to Fig. 5, the maximal phase error should be only 274° at 6.5 GHz though, based on the measurement results at 2.6 GHz and 3 GHz, this curve seems to be slightly shifted to the left for the manufactured lens.

5. CONCLUSION

A novel microwave low-reflection transmission-line lens design based on transmission lines loaded with inductive meander line elements is presented. The profile of the lens is flat and it has inhomogeneous refractive index achieved by changing the inductive loading of the transmission lines. Experimental and numerical results confirm the operation of the lens near the design frequency.

ACKNOWLEDGMENT

Some of the calculations presented above were performed using computer resources within the Aalto University School of Science "Science-IT" project.

Authors thank Mr. Lauri Laakso for help in preparing the measurement setup.

REFERENCES

1. Lo, Y. T. and S. W. Lee, *Antenna Handbook — Theory, Application, and Design*, Van Nostrand Reinhold, 1988.

2. Sato, K. and H. Ujiie, "A plate Luneberg lens with the permittivity distribution controlled by hole density," *Electronics and Communications in Japan (Part I: Communications)*, Vol. 85, No. 9, 1–12, 2002.
3. Bor, J., O. Lafond, H. Merlet, P. Le Bars, and M. Himdi, "Foam based Luneburg lens antenna at 60 GHz," *Progress In Electromagnetics Research Letters*, Vol. 44, 1–7, 2014.
4. Fuchs, B., L. Le Coq, O. Lafond, S. Rondineau, and M. Himdi, "Design optimization of multishell Luneburg lenses," *IEEE Trans. Antennas Propag.*, Vol. 55, No. 2, 283–289, 2007.
5. Rudolph, S. M., C. Pfeiffer, and A. Grbic, "Design and free-space measurements of broadband, low-loss negative-permeability and negative-index media," *IEEE Trans. Antennas Propag.*, Vol. 59, No. 8, 2989–2997, 2011.
6. Iyer, A. K. and G. V. Eleftheriades, "A multilayer negative-refractive-index transmission-line (NRI-TL) metamaterial free-space lens at X-band," *IEEE Trans. Antennas Propag.*, Vol. 55, No. 10, 2989–2997, 2007.
7. Quevedo-Teruel, O., W. Tang, R. C. Mitchell-Thomas, A. Dyke, H. Dyke, L. Zhang, S. Haq, and Y. Hao, "Transformation optics for antennas: Why limit the bandwidth with metamaterials?" *Sci. Rep.*, Vol. 3, 1903, 2013.
8. Alitalo, P., O. Luukkonen, J. Vehmas, and S. A. Tretyakov, "Impedance-matched microwave lens," *IEEE Antennas Wireless Propag. Lett.*, Vol. 7, 187–191, 2008.
9. Alitalo, P., F. Bongard, J. Mosig, and S. Tretyakov, "Transmission-line lens antenna with embedded source," *Proc. 3rd European Conference on Antennas and Propagation (EuCAP 2009)*, 625–629, Berlin, Germany, Mar. 23–27, 2009.
10. Eleftheriades, G. V. and K. G. Balmain, *Negative-refraction Metamaterials: Fundamental Principles and Applications*, Wiley, 2005.
11. Caloz, C. and T. Itoh, *Electromagnetic Metamaterials: Transmission Line Theory and Microwave Applications*, Wiley, 2006.
12. Alitalo, P., O. Luukkonen, L. Jylhä, J. Venermo, and S. A. Tretyakov, "Transmission-line networks cloaking objects from electromagnetic fields," *IEEE Trans. Antennas Propag.*, Vol. 56, No. 2, 416–424, 2008.
13. Pfeiffer, C. and A. Grbic, "A printed, broadband Luneburg lens antenna," *IEEE Trans. Antennas Propag.*, Vol. 58, No. 9, 3055–3059, 2010.
14. Pacheco-Peña, V., V. Torres, M. Navarro-Cía, M. Beruete, M. Sorolla, and N. Engheta, "ϵ-near-zero graded index structure as a bi-concave metallic lens using stacked rectangular near cut-off waveguides," *7th European Conference on Antennas and Propagation (EuCAP)*, 2535–2537, Gothenburg, Sweden, Apr. 8–12, 2013.
15. Vehmas, J., P. Alitalo, and S. A. Tretyakov, "Experimental demonstration of antenna blockage reduction with a transmission-line cloak," *IET Microwaves Antennas & Propagation*, Vol. 6, No. 7, 830–834, 2012.
16. Vehmas, J., P. Alitalo, and S. Tretyakov, "Low-reflection inhomogeneous microwave lens based on loaded transmission lines," *7th European Conference on Antennas and Propagation (EuCAP)*, 1585–1589, Gothenburg, Sweden, Apr. 8–12, 2013.
17. Alitalo, P., S. Ranvier, J. Vehmas, and S. Tretyakov, "A microwave transmission-line network guiding electromagnetic fields through a dense array of metallic objects," *Metamaterials*, Vol. 2, No. 4, 206–212, 2008.
18. Pozar, D. M., *Microwave Engineering*, 3rd Edition, Wiley, USA, 2005.
19. Poularikas, A. D., *Handbook of Formulas and Tables for Signal Processing*, CRC Press LLC, 1999.